

# FH-DRL: Exponential–Hyperbolic Frontier Heuristics with DRL for Accelerated Exploration in Unknown Environments

Seunghyeop Nam, Tuan Anh Nguyen *IEEE Member*, Eunmi Choi, Dugki Min

**Abstract**—Autonomous robot exploration in large-scale or cluttered environments remains a central challenge in intelligent vehicle applications, where partial or absent prior maps constrain reliable navigation. This paper introduces *FH-DRL*, a novel framework that integrates a customizable heuristic function for frontier detection with a Twin Delayed DDPG (TD3) agent for continuous, high-speed local navigation. The proposed heuristic relies on an exponential–hyperbolic distance score, which balances immediate proximity against long-range exploration gains, and an occupancy-based stochastic measure, accounting for environmental openness and obstacle densities in real time. By ranking frontiers using these adaptive metrics, *FH-DRL* targets highly informative yet tractable waypoints, thereby minimizing redundant paths and total exploration time. We thoroughly evaluate *FH-DRL* across multiple simulated and real-world scenarios, demonstrating clear improvements in travel distance and completion time over frontier-only or purely DRL-based exploration. In structured corridor layouts and maze-like topologies, our architecture consistently outperforms standard methods such as Nearest Frontier, Cognet Frontier Exploration, and Goal Driven Autonomous Exploration. Real-world tests with a Turtlebot3 platform further confirm robust adaptation to previously unseen or cluttered indoor spaces. The results highlight *FH-DRL* as an efficient and generalizable approach for frontier-based exploration in large or partially known environments, offering a promising direction for various autonomous driving, industrial, and service robotics tasks.

**Index Terms**—Frontier-base Exploration, Deep Reinforcement Learning, Heuristic Optimisation, Self Navigation, SLAM

## I. INTRODUCTION

Autonomous exploration in complex, uncharted environments remains a core challenge for intelligent vehicles and mobile robotics [1–3]. Despite recent advances in perception and navigation, many robotic systems still rely on partial or pre-existing maps, limiting their performance when operating in large-scale or dynamic settings. A fundamental concept to tackle this gap is *frontier-based exploration*, wherein the robot incrementally discovers environment boundaries, or “frontiers,” between known and unknown regions [4]. By continually moving toward these boundaries, frontier-based methods can, in principle, guarantee full coverage of the space. However, purely heuristic frontier selection often leads to

suboptimal or redundant paths, especially in cluttered, multi-frontier situations [5, 6]. Consequently, improvements are needed to address such inefficiencies, especially for highly dynamic or large-scale environments.

Recent developments in *deep reinforcement learning* (DRL) suggest a potential remedy, enabling robots to autonomously learn navigation policies through interactions with the environment [7, 8]. In principle, DRL-based exploration agents can surpass human-engineered heuristics by dynamically adapting to varied and unpredictable conditions. Nevertheless, purely end-to-end DRL frameworks—where the robot learns everything from raw sensor streams to action outputs—are prone to several drawbacks: (1) the search space in large unknown environments is excessively high-dimensional; (2) the training process can be extremely data-intensive and unstable; and (3) guaranteeing full coverage with end-to-end policies is challenging unless carefully designed reward mechanisms and exploration strategies are in place [2, 6]. Furthermore, standard robotic navigation stacks in ROS, such as `nav2`, generally depend on costmaps generated from partial prior knowledge and may prove inadequate in fully unknown areas.

### A. Motivation and Research Gap

Bridging the strengths of frontier-based exploration with the adaptability of DRL presents an appealing hybrid direction. Traditional frontier algorithms robustly detect unknown regions but may not effectively optimize travel distance or completion time; DRL, conversely, learns to refine movement decisions but faces difficulties when searching the entire action space in large environments. Several works have investigated this synergy, typically by letting a learning agent select frontiers or vantage points, while classical motion-planning algorithms handle low-level control [5, 9]. Despite progress, key research gaps persist:

- **Suboptimal frontier scoring:** The conventional reliance on static, distance-oriented heuristics can yield frequent revisits and overly conservative paths [4]. Balancing short-range distance efficiency with a frontier’s long-term information gain remains a challenge.
- **Lack of an adaptable, integrated framework:** Many existing solutions fix certain components—such as occupancy scoring or local planning—limiting adaptability to unforeseen map structures or dynamic obstacles. A more flexible, DRL-driven frontier scoring and selection could better handle complex layouts.

Seunghyeop Nam is with Department of Computer Science and Engineering, Konkuk University, Seoul 05029, South Korea, tomska@konkuk.ac.kr

Tuan Anh Nguyen and Dugki Min are with the Department of Artificial Intelligence, Graduate School, Konkuk University, Seoul 05029, South Korea, anhnt2407, dkmin@konkuk.ac.kr

Eunmi Choi is the School of Software, College of Computer Science, Kookmin University, Seoul 02707, South Korea, emchoi@kookmin.ac.kr

- **High-speed exploration with partial observability:** Mobile robots often face limited onboard sensing and partial maps. Methods relying heavily on global costmaps or dense sensor fusion can stagnate if those costmaps are incomplete. Meanwhile, pure DRL policies can fail to generalize or exhibit slow learning when confronted with entirely unstructured spaces.

### B. Contributions and Novelty

In this paper, we propose a novel architecture, termed *FH-DRL* (Frontier Heuristic Deep Reinforcement Learning), that combines *heuristic frontier selection* with DRL-based local navigation to address the aforementioned gaps. Our key contributions are as follows:

- 1) **Adaptive frontier identification via an exponential-hyperbolic scoring function:** We design a distance score that blends exponential and hyperbolic terms, complemented by an occupancy-based stochastic measure to prioritize frontiers effectively. This addresses limitations in classical distance- or occupancy-only methods [5, 6].
- 2) **Seamless integration of DRL into local navigation:** A Twin Delayed DDPG (TD3) controller operates continuously within the partially known map, offering robust obstacle avoidance while retaining high speeds. This mitigates slowdown issues commonly observed in standard global planners that rely on static costmaps.
- 3) **Extensive validation in simulation and real environments:** We thoroughly evaluate *FH-DRL* in ROS2 and Gazebo simulations, as well as real-world testing on a Turtlebot3 *waffle\_pi*. Comparisons against state-of-the-art frontier-based (NF, CFE) and DRL-based (GDAE) exploration methods show significant reductions in exploration time and travel distance across various complexity levels.
- 4) **Scalable approach for intelligent vehicles and beyond:** Owing to the modular combination of heuristic frontier detection and DRL-based local planning, *FH-DRL* is readily transferable to broader robotic systems, such as autonomous ground vehicles, industrial automation platforms, and planetary rovers, which operate in partially mapped or changing environments.

### C. Paper Outline

The remainder of this paper is organized as follows. Section II reviews frontier-based exploration and DRL-based approaches, highlighting recent hybrid methods. Section III details our *Frontier Heuristic Algorithm*, introducing the exponential-hyperbolic distance score and occupancy stochastic measure. Section IV describes the *FH-DRL* architecture, explaining how heuristic frontier selection and TD3-based control coalesce. In Section V, we present simulation and real-world experiments, while Section VI concludes with key insights, limitations, and avenues for future work.

## II. RELATED WORK

Research in autonomous exploration can be broadly grouped into (A) frontier-based approaches, (B) deep reinforcement

learning (DRL)-based methods, and (C) hybrid solutions that integrate classical frontier-based heuristics with learning frameworks. Table I compares representative works (including the proposed *FH-DRL*) according to their primary focus, exploration strategy, key contributions, and evaluation settings.

### A. Frontier-Based Exploration

Early pioneering work by Yamauchi [4] introduced the notion of frontiers—boundaries between known and unknown regions—for iteratively driving the robot into uncharted areas. Subsequent extensions addressed inefficiencies in original frontier detection. For example, Holz *et al.* [10] proposed clustering of frontier points to reduce computational overhead in large maps, while Basilico and Amigoni [11] introduced multi-criteria decision making to balance map coverage against task objectives. Gao *et al.* [12] and Lubanco *et al.* [5] respectively refined frontier-selection heuristics by incorporating robot heading information and clustering for managing multiple frontiers in cluttered or open corridors.

Further improvements tackle incremental or dynamic frontier detection. Keidar and Kaminka [13] proposed wavefront-based frontier detectors for faster updates, and Senarathne *et al.* [14] discussed incremental algorithms for safe and reachable frontier detection in real-time. Meanwhile, Liu *et al.* [15] introduced heuristics-biased sampling to reduce both map coverage time and repeated visits. Despite these advances, purely frontier-driven methods often lack deeper adaptive capabilities when the search space or dynamic obstacles grow more complex [16].

### B. DRL-Based Exploration

Deep reinforcement learning enables robots to learn navigation and exploration policies directly from experience, mitigating reliance on prior map information or carefully hand-engineered heuristics. Niroui *et al.* [2] demonstrated end-to-end DRL exploration in cluttered rescue environments, showing faster coverage than classical approaches but also encountering slow convergence. Peake *et al.* [7] employed DRL to adaptively switch between goal-directed and random exploration behaviors, boosting coverage under sensor noise. Cao *et al.* [8] scaled DRL to large domains via hierarchical policies, whereas Li *et al.* [17] tackled partially observable settings by introducing subgoals to guide exploration in unknown zones.

However, fully DRL-based planners risk incurring high sample complexity and difficulty in ensuring guaranteed frontier coverage. Large or complex environments can cause partial observability issues that hamper policy learning [18]. Even with advanced reward shaping [19] or intrinsic motivation [20], purely learning-driven systems can stall in local minima or repeatedly revisit certain areas unless carefully trained over extensive simulation runs [21].

### C. Hybrid Approaches: Frontier-Driven and Learning-Based

To overcome the limitations of purely heuristic frontier algorithms and purely DRL exploration, recent works have

combined the two paradigms. Cimurs *et al.* [6] introduced a goal-driven exploration strategy in which frontiers were generated in a classical manner, but the selection among candidate frontiers was refined by a learned policy. In a similar vein, Wang *et al.* [22] adopted DRL to rank frontier points, thereby improving map coverage and reducing travel distance over conventional frontier-based heuristics. Some studies incorporate advanced heuristics or cost functions—for instance, Chen *et al.* [23] explored how heuristics can guide the DRL search space, accelerating the policy’s convergence and focusing the exploration on promising frontiers.

Despite these hybrid successes, open challenges remain. Many existing solutions rely on domain-specific heuristics or single-criterion cost functions, failing to balance the trade-offs among path length, coverage, and dynamic obstacle avoidance [3, 24]. Moreover, fewer works provide *full integration* of frontier detection, local DRL-based motion planning, and continuous path re-optimization. Therefore, there exists a gap in seamlessly unifying robust frontier selection methods with an adaptive local planner that can consistently navigate around obstacles at higher speeds.

#### D. Our Contribution

The proposed *FH-DRL* architecture aligns with these hybrid approaches, yet it introduces several unique features. First, an *exponential-hyperbolic distance score* couples short-range feasibility with long-range gain, a departure from conventional distance- or occupancy-only frontier heuristics. Second, it deploys DRL (via Twin Delayed DDPG) in the *local navigation loop*, ensuring continuous obstacle avoidance without reliance on prior costmaps. Furthermore, *FH-DRL* evaluates occupancy stochastics within a customizable circular region around each frontier, catering to real-time sensor constraints. As shown later, these design decisions collectively advance exploration efficiency, coverage rate, and motion smoothness compared to existing frontier-only or purely DRL approaches.

### III. FRONTIER HEURISTIC ALGORITHM

The Frontier Heuristic Algorithm, introduced in the Way-Point Selection Node (see Figure 1), addresses the challenge

of prioritising frontier points in unknown environments by synthesising spatial and occupancy-based criteria. Specifically, the algorithm dynamically combines a distance-based score,  $\mathcal{D}(x_f, y_f)$ , and an occupancy score,  $\mathcal{O}(x_f, y_f)$ , to quantify the exploration value of each frontier, thereby minimising redundant paths and unnecessary exploration.

The distance-based score,  $\mathcal{D}(x_f, y_f)$ , is optimised to reflect the constraints of both linear and angular robot velocities. It employs a customised “exponbolic” function that adjusts the score across three intervals—close-range, proportional, and far-range distances—thus ensuring balanced evaluation over multiple scales. Concurrently, the occupancy-based score,  $\mathcal{O}(x_f, y_f)$ , interprets local grid maps to determine the proportion of unknown and obstacle-occupied cells around each frontier, factoring in both environmental openness and occupancy density.

#### Algorithm 1 Frontier Detection

---

```

1: Initialise  $\mathcal{F}$  as size of  $M$  array, filled with Non-Frontier marks
2: Set  $w$  and  $h$  as width and height of given map
3: for  $i = 0$  to  $w - 1$  and  $j = 0$  to  $h - 1$  do
4:   if  $M[i + w \cdot j]$  is  $\zeta_f$  then
5:     if  $i > 0$  and  $M[(i - 1) + w \cdot j]$  is  $\zeta_o$  then
6:        $\mathcal{F}[i + w \cdot j] \leftarrow f$ 
7:     else if  $i < w - 1$  and  $M[(i + 1) + w \cdot j]$  is  $\zeta_u$  then
8:        $\mathcal{F}[i + w \cdot j] \leftarrow f$ 
9:     else if  $j > 0$  and  $M[i + w \cdot (j - 1)]$  is  $\zeta_u$  then
10:       $\mathcal{F}[i + w \cdot j] \leftarrow f$ 
11:    else if  $j < h - 1$  and  $M[i + w \cdot (j + 1)]$  is  $\zeta_u$  then
12:       $\mathcal{F}[i + w \cdot j] \leftarrow f$ 
13:    end if
14:  end if
15: end for
16: return  $\mathcal{F}$ 

```

---

Equation 4 presents the final heuristic function,  $h(x_f, y_f)$ , which combines both scores through a tunable discount factor  $\gamma$ . Larger values of  $\mathcal{O}(x_f, y_f)$  primarily indicate open areas, whereas lower values reflect regions dominated by unknown spaces. Consequently, the algorithm favors frontiers with lower heuristic values, thereby selecting exploration objectives that effectively balance navigational efficiency with frontier exploration.

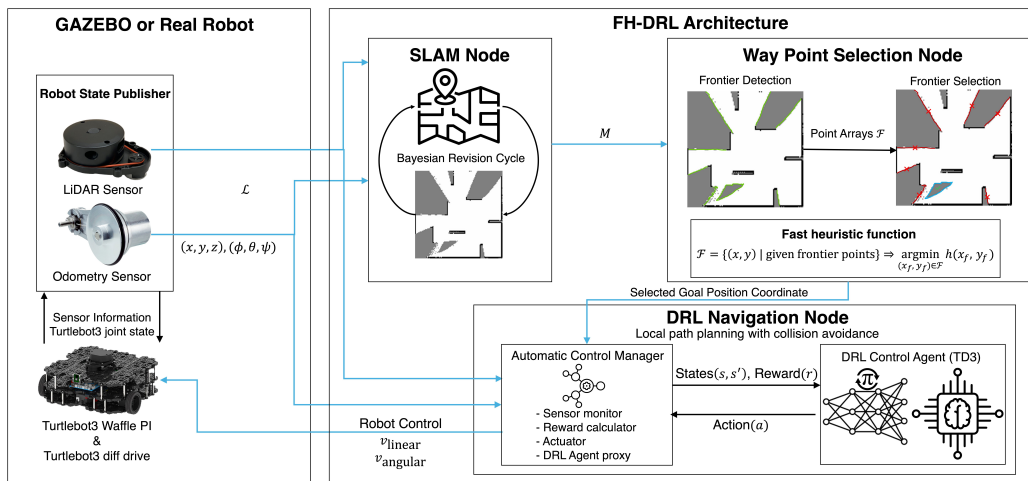


Fig. 1: Overall Robot Navigation for Exploration Architecture

TABLE I: Representative Works in Frontier-Based and Learning-Based Exploration, Contrasted with FH-DRL.

Reference	Year	Approach Type	Key Contributions	Evaluation	Focus
Yamauchi [4]	1997	Frontier-based	Foundational frontier definition	Simulation + Real	Coverage
Holz [10]	2010	Frontier-based	Frontier clustering for large maps	Simulation	Efficiency
Basilico [11]	2011	Frontier-based	Multi-criteria approach in rescue ops	Simulation	Multi-objective
Lubanco [5]	2020	Frontier-based	Clustering + utility/cost for mobile robots	Simulation	Efficiency
Niroui [2]	2019	DRL-based	DRL in complex, cluttered rescue settings	Simulation	Unstructured environ.
Peake [7]	2021	DRL-based	Adaptive exploration policy for UAV	Simulation	UAV-based
Cimurs [6]	2022	Hybrid (Frontier + DRL)	Goal-driven frontier selection w/ DRL	Simulation	Large-scale coverage
Wang [22]	2024	Hybrid (Frontier + DRL)	Deep RL ranks frontier goals	Simulation + Real	Shorter exploration paths
Fan [3]	2023	Hybrid (Edge-based + RL)	Hierarchical path planner w/ frontier RL	Simulation	Outer-planet exploration
Liu [15]	2023	Frontier-based	Heuristics-biased sampling for coverage	Simulation + Real	Efficiency
Cao [8]	2024	DRL-based	Large-scale exploration w/ hierarchical RL	Simulation	Scalability
<b>FH-DRL (Ours)</b>	<b>2024</b>	<b>Hybrid</b>	Exponential-hyperbolic frontier scoring; DRL-based local navigation (TD3); Occupancy stochastic function	Simulation + Real	Improved coverage, dynamic avoidance

### A. Frontier Detection

The frontier detection procedure, outlined in Algorithm 1, requires the occupancy grid map  $M$  from the SLAM node. The map  $M$  designates free space ( $\zeta_f$ ), obstacles ( $\zeta_o$ ), and unknown space ( $\zeta_u$ ). The detection algorithm searches for  $\zeta_u$  cells adjacent to  $\zeta_f$  or  $\zeta_o$ , expands them in eight directions, and labels them as frontier points with a value  $f$ . Ultimately, the resulting set of frontier cells  $\mathcal{F}$  is returned as an array at the conclusion of the frontier detection process.

### B. Exponential-Hyperbolic Distance Score

A straightforward linear distance metric between the robot and a frontier is inadequate because it does not account for factors such as the unknown extent of the exploration environment or the robot's limited linear and angular velocities. To address these constraints, we introduce the Exponential-Hyperbolic Distance Score, formulated in Equation 1.

$$\mathcal{D}(x_f, y_f) = \tanh \left( e^{\frac{d(x_f, y_f)}{\beta}} \cdot \sigma \left( e^{\frac{d(x_f, y_f)}{\beta}} \cdot \left( 1 - \operatorname{csch} \frac{d(x_f, y_f)}{\alpha} \right) \right) \right) \quad (1)$$

Here,  $\tanh$  and  $\operatorname{csch}$  denote the hyperbolic tangent and hyperbolic cosecant functions, respectively, while  $e$  is Euler's number. The Euclidean distance is defined as  $d(x_r, y_r) = \sqrt{(x_r - x_f)^2 + (y_r - y_f)^2}$ , where  $(x_r, y_r)$  represent the robot's coordinates and  $(x_f, y_f)$  corresponds to the centroid of the frontier. This expression interleaves exponential and hyperbolic terms, yielding a score dominated by the hyperbolic component at shorter distances and by the exponential component at longer distances. Additionally, the sigmoid normalisation  $\sigma(x) = \frac{1}{1+e^{-x}}$  confines the output to the interval  $(0, 1)$ .

The function partitions scoring into three regions:

- A region that converges to 0, mitigating the effect of small distance disadvantages.
- A region in which the score grows with distance, balancing the trade-off between distance and  $\mathcal{O}(x_f, y_f)$  (see Section III-C).
- A region that approaches 1, effectively penalising distances beyond a specified threshold.

The parameters  $\alpha$  and  $\beta$  regulate the overall behavior of the function:  $\alpha$  determines where the slope begins, whereas  $\beta$  sets

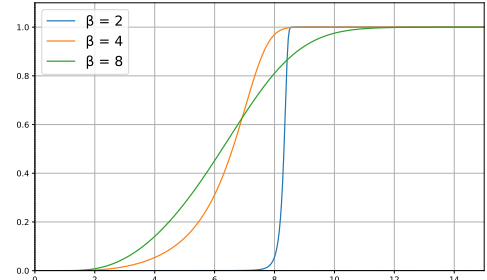


Fig. 2: Exponential-Hyperbolic Distance Score

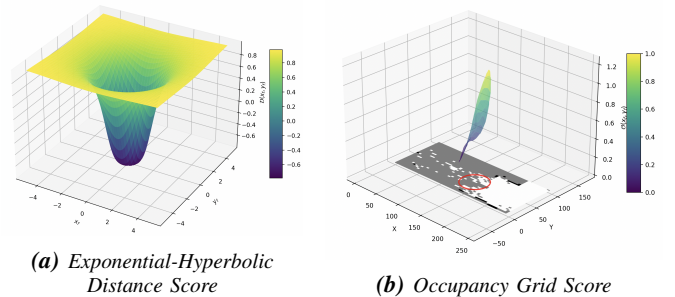


Fig. 3: Visualisation of exponential-hyperbolic distance and occupancy grid score distribution

its gradient  $\left( \frac{\partial}{\partial d} d(x_f, y_f) \right)$ . These parameters can be chosen based on the robot's LiDAR range and average speed. For example, a robot equipped with a more extensive LiDAR coverage—enabling larger map updates per Bayesian cycle—may require a higher  $\alpha$  to deprioritise frontiers at closer ranges. Conversely, a faster robot may benefit from a larger  $\beta$  to capture its enhanced capacity for reaching distant frontiers.

The equation's raw form can be difficult to deploy directly because the slope pivots near the  $\frac{1}{2}$  mark, complicating how  $\alpha$  and  $\beta$  are interpreted. To address this, an additional exponential term stabilises the function, setting the pivot at the maximal score of 1. Lastly, the  $\tanh$  normalisation ensures a smooth, bounded output. The resultant Exponential-Hyperbolic Distance Score is illustrated in Figure 2, with a 3D visualisation of the score's spatial distribution relative to the robot's location in Figure 3a.



### C. Occupancy Stochastic Score

The Occupancy Stochastic Score, as the name implies, evaluates the occupancy grid map in the vicinity of a frontier to determine its exploratory value. The score is computed according to Equation 2:

$$\mathcal{O}(x_f, y_f) = \frac{\sum_{(x,y) \in S} m(x,y)}{\pi r^2} \cdot \text{sech}(a_f), \quad (2)$$

$$S = \left\{ (x, y) \mid (x - x_f)^2 + (y - y_f)^2 \leq r^2 \right\}, \quad (3)$$

where  $\text{sech}$  is the hyperbolic secant function,  $(x_f, y_f)$  designates the centroid of the frontier, and  $a_f$  is the frontier length.  $m(x,y)$  is the occupancy value at the position  $(x,y)$ , defined over the set  $S$  in Equation 3. Unlike GDAE, which employs a discretised square kernel, the FH-DRL architecture computes continuous obstacle likelihood within a circular region, thereby enhancing stability through orientation-sensitive and smoothly probabilistic modelling that includes unknown, free, and occupied cells in the frontier.

The function  $m(x,y)$  represents the occupancy value at a given point  $(x,y)$  on the map. Within the `costmap2D` infrastructure of ROS2, inflation propagates costs outward from occupied cells with diminishing intensity proportional to the distance. We define five distinct categories of cost relevant to the robot's movement:

- "Lethal" cost indicates an actual obstacle cell with a high probability of collision at the robot's centre.
- "Inscribed" cost denotes a cell lying inside the robot's inscribed radius from an obstacle, ensuring collision if the robot's centre occupies it.
- "Possibly circumscribed" cost implies that collision may occur based on the robot's orientation.
- "Freespace" cost is zero, indicating no known obstacles.
- "Unknown" cost conveys no available information about the cell, leaving its interpretation open.

Other costs lie between "Freespace" and "Possibly circumscribed" as a function of their distance from a "Lethal" cell and a user-defined decay function. This flexible scheme allows planners to consider the robot's footprint only when orientation is critical. Each cell in the map has up to 255 probability values. By remapping 255 (unknown) to 0 and incrementing all other values by 1, unknown cells are set to 0 while those with higher obstacle likelihood obtain larger values. Cells confirmed to contain obstacles (probability 1) take on the maximum value of 255, signifying a minimal exploratory benefit. We set the radius  $r$  from the frontier centroid to its outermost frontier cell to assess the exploration value. Summing the probability values for all cells inside this circle, then dividing by the circle's area, yields an average probability in the interval  $[0, 1]$ . A value near 0 signifies predominantly unknown or free areas, whereas a value approaching 1 indicates mostly obstacle-occupied regions, which in turn lowers the exploration value. Finally, normalising these localised probability characteristics via  $\text{sech}(a_f)$  and multiplying by the frontier length yield  $\mathcal{O}(x_f, y_f)$ , which accounts for both openness and size. While

GDAE employs a fixed kernel size for evaluation—leading to potential generalisation limitations—the FH-DRL framework dynamically adjusts the inscribed circular radius, facilitating more accurate heuristic estimation. A 3D depiction of the resulting  $\mathcal{O}(x_f, y_f)$  distribution appears in Figure 3b.

### D. Frontier Types

Frontier points in the exploration space can be classified into three main categories according to their spatial configuration.

a) *Closed Frontier*: As depicted in Figure 4a, closed frontiers generally emerge between regions that have already been explored, forming gaps that remain uncharted. Giving these frontiers a higher priority enhances exploration efficiency by obviating the need for subsequent returns. Their defining elements include a red boundary denoting the frontier line, a green centroid, a yellow marker indicating the farthest point from the centroid, and a blue circle whose radius matches the distance to that yellow point. Because unknown space predominantly occupies the interior of this circle, the resulting  $\mathcal{O}(x_f, y_f)$  value tends toward 0, making it the lowest among the three frontier types.

b) *Open Wide Frontier*: Open wide frontiers occur in expansive areas perceived by the robot's LiDAR sensor, extending beyond its immediate range threshold, as illustrated in Figure 4b. Prioritising these frontiers often enhances exploration efficiency, since they typically align with the robot's primary direction of travel. Owing to a mixture of unknown cells, free space, and occasional obstacles,  $\mathcal{O}(x_f, y_f)$  is higher here than in closed frontiers, rendering them the second priority.

c) *Door Gap Frontier*: As shown in Figure 4c, door gap frontiers arise where obstacles—such as opened doors—create narrow passageways between explored areas. These frontiers commonly appear during transitions between spaces or when altering navigation paths. To promote efficiency, this type should be assigned the lowest priority if the present area remains only partially explored. Due to their relatively higher ratio of free space interspersed with some unknown zones,  $\mathcal{O}(x_f, y_f)$  reaches its maximum among the three frontier types, making it the last choice for exploration.

### E. Frontier Heuristic Function

A fast heuristic function harnesses empirical knowledge to reduce both search paths and computation time, thereby expediting and enhancing the process of finding optimal solutions. At close distances, the corresponding score converges to 0, ensuring negligible distinctions among nearby points. Beyond a certain threshold, the derivative of this function rises steeply before decreasing. Consequently,  $\mathcal{D}(x_f, y_f)$  can be subdivided into three intervals: close-range, proportional range, and far-range. By integrating the scores from  $\mathcal{D}(x_f, y_f)$  and  $\mathcal{O}(x_f, y_f)$ , one obtains the final heuristic function defined in Equation 4, whose three-dimensional distribution is depicted in Figure 5.

$$h(x_f, y_f) \equiv \mathcal{D}(x_f, y_f) \cdot \gamma + \mathcal{O}(x_f, y_f) \cdot (1 - \gamma) \quad (4)$$

In this formulation, the parameter  $\gamma$  serves as a discount factor that modulates the heuristic function under the constraint

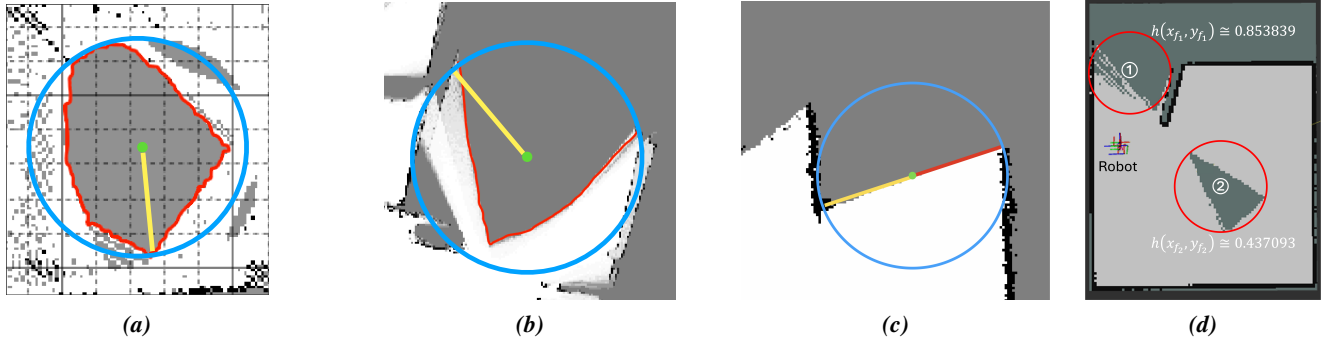


**Fig. 4: Representative Frontiers**  
 (a). Closed Frontier, (b). Open Wided Frontiers, (c). Door Gap Frontier, (d) Case-study

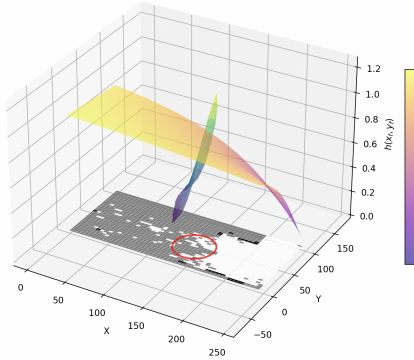


**Fig. 5: FH-DRL score 3D Distribution**

$\gamma \leq \frac{1}{2}$ . By combining distance-based and occupancy-based scores, the heuristic function determines the overall heuristic value of a given frontier point. Specifically,  $\mathcal{D}(x_f, y_f)$  is scaled by  $\gamma$ , and  $\mathcal{O}(x_f, y_f)$  is scaled by  $1 - \gamma$ . The frontier goal is then selected by minimizing this heuristic score, i.e., Frontier Goal =  $\text{argmin} h(f_i)$ , where  $f_i$  denotes the set of candidate frontier points  $(x_f, y_f)$  that integrate both distance and occupancy information for prioritizing valuable frontiers.

As illustrated in Figure 4d, consider two frontiers, Frontier 1 and Frontier 2. Frontier 1 is located between an open area and a door gap that may require further exploration. Conventional methods such as Nearest Frontier (NF), which focus primarily on proximity, would initially explore Frontier 1 and subsequently return to Frontier 2. However, under FH-DRL, Frontier 2 is prioritized due to its lower heuristic score. Its enclosed geometry, characterized by a higher ratio of unknown space and an extended frontier length, results in a reduced score. Consequently, FH-DRL avoids redundant paths by favoring Frontier 2.

## IV. FH-DRL ARCHITECTURE

### A. Overall Architecture

The FH-DRL (Frontier Heuristic Deep Reinforcement Learning) architecture, depicted in Figure 1, is designed to facilitate autonomous navigation in a GAZEBO simulation by integrating several pivotal components. The Robot State

Publisher provides essential data derived from a LiDAR sensor scanning  $n(\mathcal{L}) = 360$  at  $2\pi$  radians, along with odometry tracking ( $\text{Pose} : x, y, z; \phi, \theta, \psi$ ) and joint states. The SLAM node concurrently updates the map via a Bayesian Revision Cycle. The Way-Point Selection node identifies unexplored regions, generates arrays of candidate points, and applies a heuristic function ( $\mathcal{F} = h(x_f, y_f)$ ) to define local goals from the SLAM-generated map. Local path planning and collision avoidance fall under the DRL Navigation Node, which employs a TD3-based control agent for decision-making grounded in states  $(s, s')$ , rewards  $(r)$ , and actions  $(a)$ . The Automatic Control Manager processes sensor data for reward calculation and issues linear and angular velocity commands to the robot, facilitating both obstacle avoidance and goal-directed maneuvers. This architecture effectively integrates SLAM, frontier detection and selection, and deep reinforcement learning to achieve efficient autonomous navigation.

### B. Way-Point Selection Node

The Way-Point Selection node determines feasible exploration targets by examining frontiers within the map  $\mathcal{M}$ , as described in Section III. Once the SLAM node provides  $\mathcal{M}$ , the algorithm extracts the frontiers, which define the boundaries between known and unknown regions. By integrating distance-based and occupancy-based scores, the heuristic function prioritises unexplored areas for each frontier. Specifically, the frontier score is computed from Equation 4, which balances the distance component  $\mathcal{D}(x_f, y_f)$  against the occupancy score  $\mathcal{O}(x_f, y_f)$  according to the heuristic parameters. The frontier exhibiting the lowest heuristic value is then chosen as the robot's next waypoint, thereby optimising the trade-off between exploration speed and safety.

### C. SLAM Node

Simultaneous Localisation and Mapping (SLAM) is essential for autonomous robot navigation while enabling real-time map building and localisation. In this study, the SLAM node uses the `nav2` package in ROS2 to construct an occupancy grid which representing navigable areas and obstacles based on LiDAR sensor data.

SLAM iteratively refines the map and the robot's position by combining sensor data with motion estimates through a

Bayesian revision cycle. The Adaptive Monte Carlo Localisation (AMCL) algorithm utilises particle filters to further enhance positional accuracy. The `nav2` package integrates exploration and localisation using algorithms such as `gmapping` ensures up-to-date map generation for precise navigation in dynamic environments.

The SLAM node communicates the information to the Frontier Selection node to enable the selection of optimal exploration points for continued navigation and efficient environment coverage as soon as the updated map is generated.

#### D. DRL Navigation Node

Deep reinforcement learning (DRL) facilitates local navigation that adapts continuously to unexpected obstacles, circumventing the limitations of conventional methods such as `nav2` in ROS2—which generally rely on pre-established maps. Through active interaction with the environment, DRL methods learn navigation policies that improve adaptability, obstacle avoidance, and maximum traversal speed, even in the absence of a map. This flexibility makes DRL a compelling alternative for enhancing autonomous navigation capabilities.

The Twin Delayed DDPG (TD3) algorithm, developed by Fujimoto *et al.* [25], refines Deep Deterministic Policy Gradient (DDPG) by mitigating value overestimation in continuous action spaces, rendering it well-suited for self-navigation scenarios. Key innovations in TD3 include Clipped Double Q-learning, Delayed Policy Updates, and Target Policy Smoothing, all of which bolster its performance.

The Automatic Control Manager receives sensor data from GAZEBO and augments it with the robot’s previous actions. It then computes the reward and supplies both current and subsequent states to the TD3 agent. The actor uses the state vector ( $s_t$ ) to determine two-dimensional continuous actions, ( $A_{\text{linear}}, A_{\text{angular}}$ ). Meanwhile, during training, the critics receive the same input as the actor for their first fully connected layer, then incorporate the current-step actions in the second layer to generate Q-values.

## V. EXPERIMENTS

### A. Simulation Setup

1) *Scenario Settings*: We conducted comparative evaluations in a ROS2 and GAZEBO `Classic` environment using a `Turtlebot3 waffle_pi`. The experimental scenarios are as follows. In Scenario I (Low Complexity Map, see Figure 6b), the robot navigates a small enclosed area with internal walls. Scenario II (Medium Complexity Map, see Figure 6c) tests its ability to traverse corridors containing turns and junctions, representative of indoor office-type settings. Scenario III (High Complexity Map, see Figure 6d) introduces a maze-like layout with narrow passages, challenging advanced navigation and decision-making algorithms.

We compared frontier selection in FH-DRL against CFE [5], GDAE [6], and NF [4]. For local navigation, FH-DRL uses ROS2’s `nav2`. In order to isolate and compare only the frontier-selection capabilities, we replaced the original local path-planning component in GDAE (which was designed to reach a global goal in unknown space) with `nav2`, omitting the

TABLE II: Hyperparameter Values

Parameter	Value
Neurons in actor network	3394
Neurons in critic network	1026
Batch size	512
Buffer size	1000000
Discount factor	0.99
Learning rate	0.002
Tau	0.003
Step time	0.01
Epsilon decay	0.9995
Epsilon minimum	0.05
Policy noise	0.2
Policy noise clip	0.5
Policy update frequency	2

global goal from its heuristic function. Moreover, we evaluated FH-DRL both with and without the DRL navigation node: FH-DRL without DRL uses `nav2` for local control, whereas FH-DRL with DRL employs the proposed TD3-based controller. This setup enables an assessment of the impact of FH-DRL’s Frontier Heuristic (introduced in Section III) independent of any benefits from DRL-based navigation.

2) *Neural Networks and Hyperparameter Settings*: The actor network depicted in Table II is implemented as a fully connected neural network (FCNN) with six hidden layers, whereas the critic network consists of three hidden layers. The actor processes normalized LiDAR sensor inputs, denoted by  $n(\mathcal{L}) = 360$  and rescaled to the interval  $[0, 1]$ , in addition to state inputs such as the initial goal distance  $d_{g_{\text{init}}}$ , goal orientation  $\angle g_{\text{angle}}$ , and previous linear and angular actions,  $A_{\text{linear}}^{t-1}$  and  $A_{\text{angular}}^{t-1}$ . The critic uses these same state inputs, with its second fully connected layer also incorporating the actor’s actions ( $A_{\text{linear}}$  and  $A_{\text{angular}}$ ) to compute Q-values. Based on these estimated Q-values, the actor ultimately outputs the optimal linear and angular actions. Table II details the hyperparameters employed during training.

3) *Model Training*: The TD3 algorithm for local navigation was implemented in a GAZEBO simulation featuring six dynamic obstacles. The training spanned 10,000 episodes, conducted on a system equipped with an Intel i5-10400F CPU and an NVIDIA 3070 GPU, and required approximately two days to complete. Goals were randomly generated through the GAZEBO goal generator and forwarded to the DRL navigation node. As illustrated in Figure 6a, the training environment incorporates both static and dynamic obstacles, simulating complex navigation tasks. Training progress is visualized in Figure 7.

At the start of each episode, the robot is initialized either at the central area of the environment or at the previous goal location. Upon receiving a randomly generated goal, the robot proceeds to navigate while avoiding obstacles. An episode concludes unsuccessfully if the robot collides with an obstacle or exceeds its allotted time, triggering a penalty. By contrast, successful goal completion results in a positive reward, in accordance with Algorithm 2, thereby incentivizing faster goal attainment.

The TD3 reward function presented in Algorithm 2 integrates various criteria to guide exploration in unknown

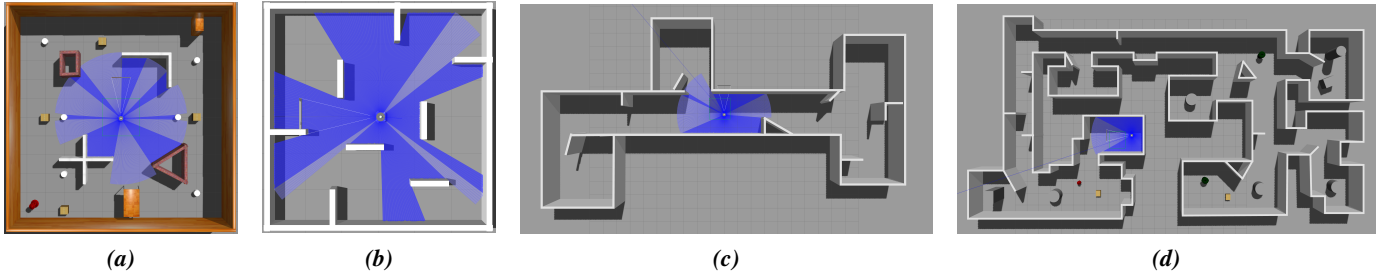


Fig. 6: Simulation Scenarios. (a) Training Environment; (b) Small Space with Obstacles; (b) Corridor with Turns; (c) Complex Maze

environments, rewarding both obstacle avoidance and efficient goal-reaching behavior. Positive rewards are issued if the Euclidean distance to the goal ( $d_{g_{\text{robot}}}$ ) is less than the initial distance ( $d_{g_{\text{init}}}$ ) or is within the threshold  $T_g$ . Penalties arise if the robot fails to maintain its maximum linear velocity ( $M_{\text{linear}}$ ), minimum angular action ( $A_{\text{angular}}$ ), or a suitable orientation ( $\angle g_{\text{angle}}$ ). Additional penalties occur whenever  $\min_{l \in \mathcal{L}} l$ —where  $l \in \mathcal{L}$ —falls below the collision threshold ( $T_c$ ) or below  $1.5 \cdot T_c$  if the robot is dangerously close to a potential collision zone.

#### Algorithm 2 Reward Function of DRL Algorithm

```

1:  $r_{\text{yaw}} \leftarrow -|\angle g_{\text{angle}}|$ 
2:  $r_{\text{linear}} \leftarrow -((M_{\text{linear}} - A_{\text{linear}}) \cdot 10)^2$ 
3:  $r_{\text{angular}} \leftarrow -A_{\text{angular}}^2$ 
4:  $r_{\text{distance}} \leftarrow \frac{d_{g_{\text{init}}} + d_{g_{\text{robot}}} - 1}{2 \cdot d_{g_{\text{init}}}}$ 
5: if  $\min_{l \in \mathcal{L}} l < 1.5 \cdot T_c$  then
6:    $r_{\text{obstacle}} \leftarrow -50$ 
7: else
8:    $r_{\text{obstacle}} \leftarrow 0$ 
9: end if
10:  $R \leftarrow \sum \{r_{\text{yaw}}, r_{\text{angular}}, r_{\text{distance}}, r_{\text{obstacle}}\}$ 
11: if  $d_{g_{\text{robot}}} < T_g$  then
12:    $R \leftarrow R + 5000$ 
13: end if
14: if  $\min_{l \in \mathcal{L}} l < T_c$  then
15:    $R \leftarrow R - 2000$ 
16: end if
17: return  $R$ 

```

### B. Experimental Simulation Results and Analyses

1) *Environment Reveal*: Table III compares the performance of multiple autonomous exploration methods across different experimental scenarios. The primary metrics encompass average, maximum, minimum, and standard deviation ( $\sigma$ ) values for distance (d, in meters), time (T, in seconds), and exploration rate (ExpR, in percent). Each scenario was evaluated by running 10 independent trials.

a) *Scenario I (Low Complexity Map)*:: FH-DRL without DRL achieves the most favorable results, with an average distance of 13.15 m and a completion time of 71.2 s. Moreover, it exhibits notably low variance in travel distance (0.67 m). FH-DRL with DRL performs comparably well (16.66 m, 81.28 s) and attains a high exploration rate (98.03%). While Nearest Frontier (NF) and Cognet Frontier Exploration (CFE) also yield high exploration rates (98.37% and 98.69%, respectively), they require significantly greater distances and times—15.47 m and 135.27 s for NF, and 22.16 m and 123.06 s

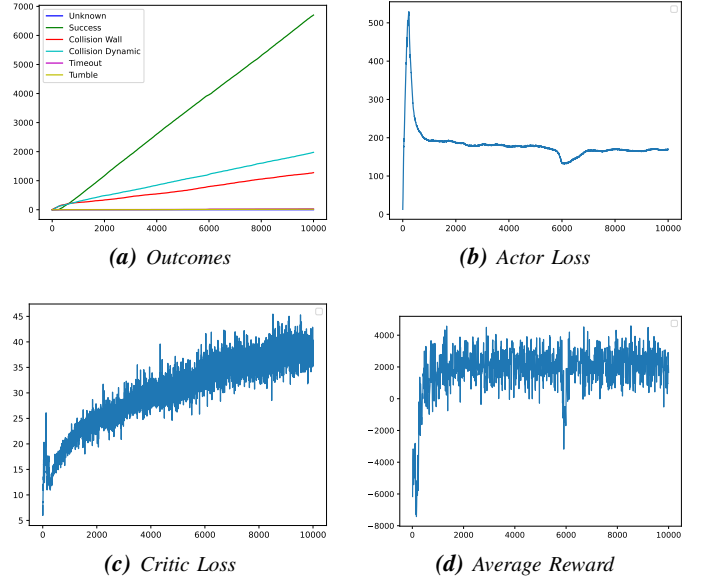


Fig. 7: Training Progress

for CFE. By contrast, GDAE exhibits the longest average time (153.47 s) and a relatively high mean distance (16.96 m), despite maintaining a comparable exploration rate (98.25%).

b) *Scenario II (Medium Complexity Map)*:: FH-DRL with DRL outperforms the alternatives by achieving the shortest average completion time (325.09 s) and a high exploration rate (99.47%). Although its average distance (76.75 m) slightly exceeds that of FH-DRL without DRL (69.48 m), the latter also offers strong performance (352.70 s, 99.24%). In contrast, NF and CFE both require substantially longer times: 542.69 s and 545.52 s, respectively. GDAE exhibits a high degree of variability, posting an average time of 880.59 s and a distance of 78.61 m.

c) *Scenario III (High Complexity Map)*:: FH-DRL with DRL again emerges as the leading approach, posting the shortest average time (785.34 s) and the highest exploration rate (99.74%). Its average distance (175.77 m) remains well below those recorded by NF and CFE. Meanwhile, FH-DRL without DRL also achieves solid results (889.19 s, 99.56%). In comparison, NF (2610.87 s, 210.73 m) and CFE (1552.86 s, 268.33 m) demand notably higher times and distances. Although GDAE covers a shorter distance (211.40 m), it records an exceptionally long average time (1251.90 s). Taken together, these findings confirm that FH-DRL, both with and without DRL, substantially outperforms the other methods—particularly in

TABLE III: Experimental Results in Completing Environment Exploration

Metrics	NF			CFE			GDAE			FH-DRL w/o DRL			FH-DRL w/ DRL		
	I	II	III	I	II	III	I	II	III	I	II	III	I	II	III
Avg dist.(m)	15.471	83.897	210.731	22.162	91.692	268.330	16.958	78.611	211.397	13.151	69.480	163.879	16.655	76.745	175.768
Min dist.(m)	13.027	71.441	180.311	19.357	80.325	210.376	13.806	68.933	187.847	12.170	61.677	153.073	16.655	67.926	161.479
Max dist.(m)	17.540	95.460	244.956	25.998	104.449	337.185	20.388	91.310	267.180	13.985	80.995	188.797	20.531	87.555	194.186
$\sigma$ (dist)	1.840	8.057	21.329	2.418	7.630	31.981	2.039	8.161	23.593	0.667	5.280	10.566	2.717	7.150	12.324
Avg T.(sec)	135.270	542.690	2610.870	123.060	545.520	1552.860	153.470	880.590	1251.900	71.200	352.700	889.190	81.280	325.090	785.340
Min T.(sec)	111.900	487.100	1115.100	109.400	490.200	1277.800	107.900	354.800	1051.600	58.600	310.100	804.100	66.100	276.700	683.100
Max T.(sec)	151.400	670.200	14167.100	140.500	588.100	1764.900	253.600	4545.000	1600.300	86.100	409.200	1019.400	99.700	382.200	870.000
$\sigma$ (T)	13.887	53.853	4063.987	12.147	37.931	167.475	39.445	1290.434	163.315	10.469	30.809	77.790	11.924	37.995	63.175
Avg ExpR.(%)	98.370	99.485	99.099	98.688	99.423	98.981	98.247	99.495	98.971	97.784	99.240	99.557	98.025	99.466	99.735
Min ExpR.(%)	97.501	99.165	95.272	98.261	99.230	95.249	98.010	99.112	97.116	97.486	97.478	99.236	96.453	99.042	99.539
Max ExpR.(%)	99.134	99.866	99.894	99.947	99.697	99.971	98.709	99.738	99.972	98.041	99.996	99.956	99.719	99.880	99.988
$\sigma$ (ExpR)	0.502	0.244	1.463	0.594	0.134	1.944	0.176	0.189	1.128	0.002	0.670	0.190	0.882	0.260	0.123

environments of greater complexity.

2) *Distance by Time*: Figures 8a, 8b, and 8c depict the distance traveled as a function of time for GDAE, NF, CFE, FH-DRL with DRL, and FH-DRL without DRL across unknown environments (Scenarios I, II, and III). The shaded regions represent variance, reflecting the reliability of each method. In Scenario I, FH-DRL with DRL attains the lowest distances and completion times, closely followed by FH-DRL without DRL. CFE exhibits moderate performance, while NF and GDAE demonstrate less efficiency. As complexity increases (Scenarios II and III), FH-DRL with DRL continues to outperform its counterparts by completing tasks more rapidly and efficiently. Overall, FH-DRL consistently provides superior performance—particularly in complex environments—emphasising its effectiveness in exploration tasks.

3) *Exploration Rate by Distance*: Figures 8d, 8e, and 8f illustrate the relationship between exploration rate and distance. In Scenario I, NF achieves a high exploration rate over relatively short distances. In the more challenging Scenarios II and III, FH-DRL (both with and without DRL) demonstrates a noticeable performance boost and surpasses other methods. Specifically, in Scenario III, FH-DRL with DRL proves the most efficient, achieving high exploration rates with minimal traveled distance. By contrast, CFE, GDAE, and NF display lower performance, while FH-DRL excels in more intricate environments.

4) *Exploration Rate by Time*: Figures illustrating exploration rate over time for the five approaches in Scenarios I, II, and III reveal that FH-DRL with DRL swiftly reaches approximately 80% coverage within the first 20 seconds in Scenario I, followed by FH-DRL without DRL. In Scenarios II and III, FH-DRL with DRL maintains its advantage by achieving higher exploration rates in shorter time spans, again outpacing FH-DRL without DRL. CFE demonstrates moderate progress, while NF and GDAE lag behind. Taken together, these results indicate that integrating DRL substantially enhances the exploration efficiency of FH-DRL.

5) *Exploration Rate by Distance and Time*: Figures 8j–8l present three-dimensional plots relating exploration rate to both distance and time. FH-DRL (with and without DRL) not only covers greater distances in less time but also maintains high exploration rates in all scenarios. In contrast, GDAE, NF, and CFE face challenges over longer distances and durations, whereas FH-DRL consistently achieves more rapid and com-

prehensive exploration.

6) *Traversed Paths*: Figure 10 illustrates the robot trajectories for each method across three map complexities. FH-DRL with DRL attains the most efficient paths, characterized by minimal redundancy, while FH-DRL without DRL shows moderate retracing. NF and CFE present multiple overlapping routes, and although GDAE performs better than these two, it still falls short of FH-DRL. Notably, the DRL-based FH-DRL exhibits the highest path efficiency, especially under Scenario III.

7) *Discussion*: FH-DRL without DRL produces the shortest average travel distances, whereas FH-DRL with DRL attains the lowest average completion times, indicating more rapid exploration. Both variants maintain consistently high exploration rates with minimal variance. Leveraging both heuristic frontier selection and DRL-based navigation proves highly effective in unknown environments, outperforming competing approaches that depend on nav2-based planning and discrete movement. By integrating continuous navigation through DRL with a heuristic frontier-selection mechanism, FH-DRL achieves comprehensive map coverage in reduced time, thereby demonstrating particular promise for autonomous exploration tasks.

### C. Real-World Experiments

A real-world evaluation was performed using a Turtlebot3 waffle\_pi in a structured indoor hallway, as shown in Figure 9. This environment includes both straight and cornered sections, along with randomly placed box obstacles, thereby testing the robot’s navigation and decision-making capabilities. The narrow corridor junction further challenges path-planning algorithms, while the confined layout and features provide a rigorous testbed for the proposed FH-DRL algorithm under realistic conditions. The experimental progression is illustrated in Figure 11, highlighting the frontier-exploration process in an actual setting.

In Figure 11a, the algorithm initially selects the largest frontier based on both proximity and  $\mathcal{O}(x_f, y_f)$ . Figure 11b demonstrates the selection of a **closed frontier** which might otherwise have been overlooked if frontier size alone were considered. Figure 11c underscores a preference for an **open wide frontier** over a nearer **door gap** frontier, thereby expanding exploration opportunities. In Figure 11d, a frontier is chosen based on  $\mathcal{D}(x_f, y_f)$  to minimise exploration time,



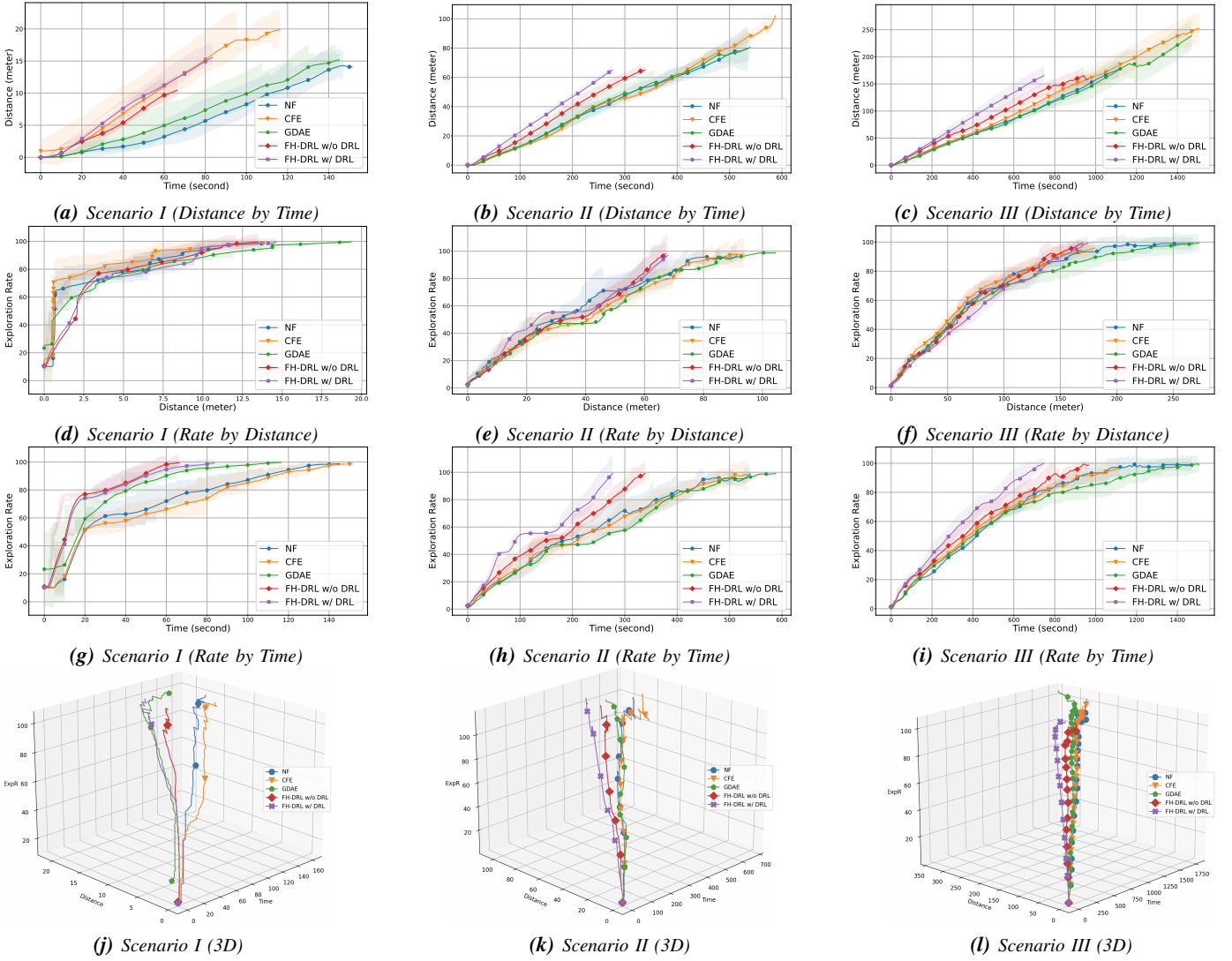


Fig. 8: Experimental Simulation Results of Robot Exploration in Unknown Spaces

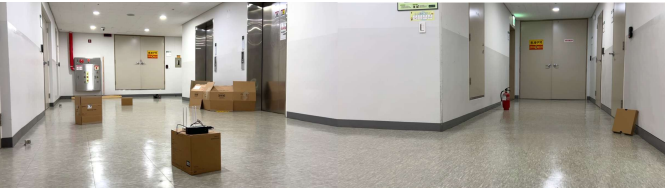


Fig. 9: Real World Experiment Environment

even though an alternative frontier has a lower  $\mathcal{O}(x_f, y_f)$ . Figure 11e highlights the robot's decision to pursue a **closed frontier**, ensuring full coverage while avoiding the need to revisit the area in the future. Lastly, Figure 11f indicates that the exploration has been successfully completed.

The corresponding experimental results, displayed in Figure 11g and Table IV, illustrate that **FH-DRL with DRL** surpasses all other frontier-based exploration algorithms in both time and distance metrics.

In terms of time efficiency, *FH-DRL with DRL* achieves the shortest exploration duration at **132.3 s**, significantly outper-

TABLE IV: Performance Comparison on Real World

Method	Time (s)	Distance (m)
NF	298.4	32.2237
CFE	423.2	33.7278
GDAE	179.5	24.5279
FH-DRL w/o DRL	172.1	23.8355
FH-DRL w/ DRL	132.3	22.85

forming its nearest competitor, FH-DRL without DRL, and far exceeding traditional methods such as CFE and NF. In parallel, *FH-DRL with DRL* also records the shortest travel distance (**22.85 m**), highlighting its superiority over FH-DRL without DRL as well as other algorithms including GDAE, CFE, and NF.

These findings underscore the robustness of the proposed algorithm, which employs DRL-based navigation to optimize path planning without relying on a static map and thus enabling efficient exploration even in cluttered environments.



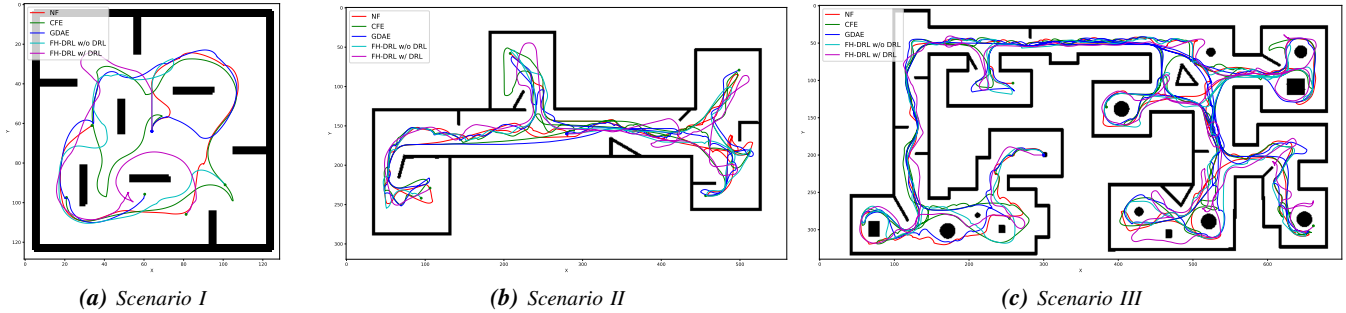


Fig. 10: Exploration paths

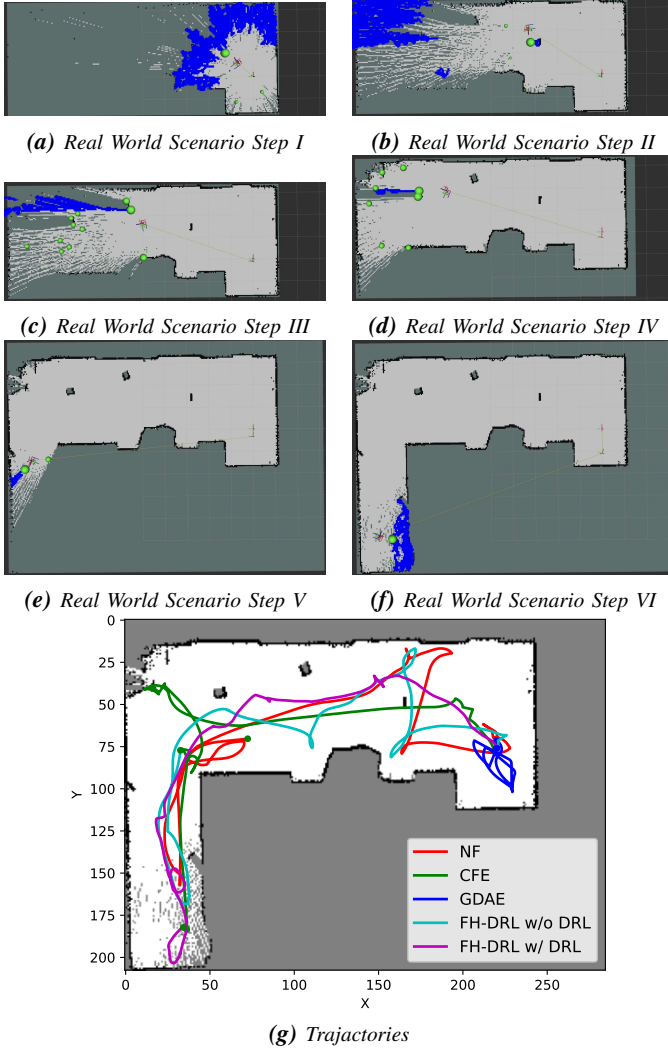


Fig. 11: Real World Experiment Phases in Unknown Spaces

## VI. CONCLUSION

In this work, we have proposed an integrated FH-DRL architecture that unites heuristic optimization with DRL, substantially enhancing exploration efficiency. Across three distinct experimental scenarios of varying complexity, FH-DRL integrated with DRL consistently achieved the highest exploration rates and shortest completion times, outperforming both classical and advanced frontier-based methods. This outcome

demonstrates the potential of combining heuristic approaches with DRL to optimize autonomous navigation, establishing FH-DRL as a promising solution for robotic exploration tasks.

The FH-DRL framework is highly scalable and adaptable, offering robust exploration solutions for applications in autonomous driving, industrial robotics, and space exploration. Empirical evidence confirms FH-DRL as an effective, innovative approach for a range of industrial settings. Future research efforts will focus on refining heuristic functions and incorporating additional sensor modalities to further strengthen robustness and adaptability.

## ACKNOWLEDGMENT

This research was supported by Basic Science Research Program through the National Research Foundation of Korea(NRF) funded by the Ministry of Education (No. 2020R1A6A1A03046811) and (2021R1A2C2094943). This paper was supported by Korea Institute for Advancement of Technology (KIAT) grant funded by the Korea Government(MOTIE) (P0020536, HRD Program for Industrial Innovation).

## REFERENCES

- [1] Z. Sun *et al.*, “Multi-Risk-RRT: An Efficient Motion Planning Algorithm for Robotic Autonomous Luggage Trolley Collection at Airports,” *IEEE Transactions on Intelligent Vehicles*, vol. 9, no. 2, pp. 3450–3463, 2024, ISSN: 2379-8904. DOI: 10.1109/TIV.2023.3349171 (cit. on p. 1).
- [2] F. Niroui, K. Zhang, Z. Kashino, and G. Nejat, “Deep Reinforcement Learning Robot for Search and Rescue Applications: Exploration in Unknown Cluttered Environments,” *IEEE Robotics and Automation Letters*, vol. 4, no. 2, pp. 610–617, 2019, ISSN: 2377-3766. DOI: 10.1109/LRA.2019.2891991 (cit. on pp. 1–2, 4).
- [3] J. Fan, X. Zhang, and Y. Zou, “Hierarchical path planner for unknown space exploration using reinforcement learning-based intelligent frontier selection,” *Expert Systems with Applications*, vol. 230, p. 120630, 2023, ISSN: 09574174. DOI: 10.1016/j.eswa.2023.120630 (cit. on pp. 1, 3–4).

- [4] B Yamauchi, “A frontier-based approach for autonomous exploration,” in *Proceedings 1997 IEEE International Symposium on Computational Intelligence in Robotics and Automation CIRA'97. Towards New Computational Principles for Robotics and Automation*, IEEE Comput. Soc. Press, 1997, pp. 146–151, ISBN: 0-8186-8138-1. DOI: 10.1109/CIRA.1997.613851 (cit. on pp. 1–2, 4, 7).
- [5] D. L. da Silva Lubanco, M. Pichler-Scheder, and T. Schlechter, “A Novel Frontier-Based Exploration Algorithm for Mobile Robots,” in *2020 6th International Conference on Mechatronics and Robotics Engineering (ICMRE)*, IEEE, 2020, pp. 1–5, ISBN: 978-1-7281-5739-9. DOI: 10.1109/ICMRE49073.2020.9064866 (cit. on pp. 1–2, 4, 7).
- [6] R. Cimurs, I. H. Suh, and J. H. Lee, “Goal-Driven Autonomous Exploration Through Deep Reinforcement Learning,” *IEEE Robotics and Automation Letters*, vol. 7, no. 2, pp. 730–737, 2022, ISSN: 2377-3766. DOI: 10.1109/LRA.2021.3133591 (cit. on pp. 1–4, 7).
- [7] A. Peake, J. McCalmon, Y. Zhang, D. Myers, S. Alqah-tani, and P. Pauca, “Deep Reinforcement Learning for Adaptive Exploration of Unknown Environments,” in *2021 International Conference on Unmanned Aircraft Systems (ICUAS)*, IEEE, 2021, pp. 265–274, ISBN: 978-1-6654-1535-4. DOI: 10.1109/ICUAS51884.2021.9476756 (cit. on pp. 1–2, 4).
- [8] Y. Cao, R. Zhao, Y. Wang, B. Xiang, and G. Sartoretto, “Deep Reinforcement Learning-Based Large-Scale Robot Exploration,” *IEEE Robotics and Automation Letters*, vol. 9, no. 5, pp. 4631–4638, 2024, ISSN: 2377-3766. DOI: 10.1109/LRA.2024.3379804 (cit. on pp. 1–2, 4).
- [9] Y. Xu *et al.*, “Explore-Bench: Data Sets, Metrics and Evaluations for Frontier-based and Deep-reinforcement-learning-based Autonomous Exploration,” in *2022 International Conference on Robotics and Automation (ICRA)*, IEEE, 2022, pp. 6225–6231, ISBN: 978-1-7281-9681-7. DOI: 10.1109/ICRA46639.2022.9812344 (cit. on p. 1).
- [10] D. Holz, N. Basilico, F. Amigoni, and S. Behnke, “Evaluating the Efficiency of Frontier-based Exploration Strategies,” in *ISR 2010 (41st International Symposium on Robotics) and ROBOTIK 2010 (6th German Conference on Robotics)*, 2010, pp. 1–8 (cit. on pp. 2, 4).
- [11] N. Basilico and F. Amigoni, “Exploration strategies based on multi-criteria decision making for searching environments in rescue operations,” *Autonomous Robots*, vol. 31, no. 4, pp. 401–417, 2011, ISSN: 0929-5593. DOI: 10.1007/s10514-011-9249-9 (cit. on pp. 2, 4).
- [12] W. Gao, M. Booker, A. Adiwahono, M. Yuan, J. Wang, and Y. W. Yun, “An improved Frontier-Based Approach for Autonomous Exploration,” in *2018 15th International Conference on Control, Automation, Robotics and Vision (ICARCV)*, IEEE, 2018, pp. 292–297, ISBN: 978-1-5386-9582-1. DOI: 10.1109/ICARCV.2018.8581245 (cit. on p. 2).
- [13] M. Keidar and G. A. Kaminka, “Robot exploration with fast frontier detection: theory and experiments,” in *Proceedings of the 11th International Conference on Autonomous Agents and Multiagent Systems - Volume 1*, ser. AAMAS '12, Richland, SC: International Foundation for Autonomous Agents and Multiagent Systems, 2012, pp. 113–120, ISBN: 0981738117 (cit. on p. 2).
- [14] P. Senarathne and D. Wang, “Incremental algorithms for Safe and Reachable Frontier Detection for robot exploration,” *Robotics and Autonomous Systems*, vol. 72, pp. 189–206, 2015, ISSN: 09218890. DOI: 10.1016/j.robot.2015.05.009 (cit. on p. 2).
- [15] J. Liu, Y. Lv, Y. Yuan, W. Chi, G. Chen, and L. Sun, “An Efficient Robot Exploration Method Based on Heuristics Biased Sampling,” *IEEE Transactions on Industrial Electronics*, vol. 70, no. 7, pp. 7102–7112, 2023, ISSN: 0278-0046. DOI: 10.1109/TIE.2022.3203762 (cit. on pp. 2, 4).
- [16] M. Juliá, A. Gil, and O. Reinoso, “A comparison of path planning strategies for autonomous exploration and mapping of unknown environments,” *Autonomous Robots*, vol. 33, no. 4, pp. 427–444, 2012. DOI: 10.1007/s10514-012-9298-8 (cit. on p. 2).
- [17] H. Li, Q. Zhang, and D. Zhao, “Deep Reinforcement Learning-Based Automatic Exploration for Navigation in Unknown Environment,” *IEEE Transactions on Neural Networks and Learning Systems*, vol. 31, no. 6, pp. 2064–2076, 2020, ISSN: 2162-237X. DOI: 10.1109/TNNLS.2019.2927869 (cit. on p. 2).
- [18] D. Mansfield and A. Montazeri, “A survey on autonomous environmental monitoring approaches: towards unifying active sensing and reinforcement learning,” *Frontiers in Robotics and AI*, vol. 11, 2024, ISSN: 2296-9144. DOI: 10.3389/frobt.2024.1336612 (cit. on p. 2).
- [19] X. Yan, J. Huang, K. He, H. Hong, and D. Xu, “Autonomous exploration through deep reinforcement learning,” *Industrial Robot: the international journal of robotics research and application*, vol. 50, no. 5, pp. 793–803, 2023, ISSN: 0143-991X. DOI: 10.1108/IR-12-2022-0299 (cit. on p. 2).
- [20] A. Feng, Y. Xie, Y. Sun, X. Wang, B. Jiang, and J. Xiao, “Efficient Autonomous Exploration and Mapping in Unknown Environments,” *Sensors*, vol. 23, no. 10, p. 4766, 2023, ISSN: 1424-8220. DOI: 10.3390/s23104766 (cit. on p. 2).
- [21] Z. Li, J. Xin, and N. Li, “End-to-End Autonomous Exploration for Mobile Robots in Unknown Environments through Deep Reinforcement Learning,” in *2022 IEEE International Conference on Real-time Computing and Robotics (RCAR)*, IEEE, 2022, pp. 475–480, ISBN: 978-1-6654-6983-8. DOI: 10.1109/RCAR54675.2022.9872253 (cit. on p. 2).
- [22] R. Wang, J. Zhang, M. Lyu, C. Yan, and Y. Chen, “An improved frontier-based robot exploration strategy

combined with deep reinforcement learning,” *Robotics and Autonomous Systems*, vol. 181, p. 104783, 2024, ISSN: 09218890. DOI: 10.1016/j.robot.2024.104783 (cit. on pp. 3–4).

- [23] C.-A. Cheng, A. Kolobov, and A. Swaminathan, “Heuristic-guided reinforcement learning,” in *Proceedings of the 35th International Conference on Neural Information Processing Systems*, ser. NIPS ’21, Red Hook, NY, USA: Curran Associates Inc., 2021, ISBN: 9781713845393 (cit. on p. 3).
- [24] R. Cimurs, I. H. Suh, and J. H. Lee, “Information-Based Heuristics for Learned Goal-Driven Exploration and Mapping,” in *2021 18th International Conference on Ubiquitous Robots (UR)*, IEEE, 2021, pp. 571–578, ISBN: 978-1-6654-3899-5. DOI: 10.1109/UR52253.2021.9494668 (cit. on p. 3).
- [25] S. Fujimoto, H. van Hoof, and D. Meger, “Addressing function approximation error in actor-critic methods,” 2018. arXiv: 1802.09477 [cs.AI] (cit. on p. 7).



**Dugki Min** received a B.S. degree in industrial engineering from Korea University in 1986, an M.S. degree in 1991 and a Ph.D. degree in 1995, both in computer science from Michigan State University. He is currently a Professor in Department of Computer Science and Engineering at Konkuk University. His research interests include cloud computing, distributed and parallel processing, big data processing, intelligent processing, software architecture, and modelling and simulation.



**Seunghyeop Nam** is a undergraduate researcher of computer science in Konkuk University Seoul Korea. He is in Distributed Multimedia Systems Laboratory (DMS Lab) at Konkuk University since 2021. His interests of research are deep reinforcement learning, robotic mechatronics, sensor fusion, vision deep learning and path planning of mobile robot.



**Tuan Anh Nguyen** (Ph.D.’15, M.Sc.’10, B.Eng.’08) is an Academic Research Professor at Konkuk University’s Aerospace Design-Airworthiness Institute in Seoul, South Korea. He is a member of IEEE, IEEE Computer, Robotics and Automation (IEEE RAS), Aerospace and Electronic Systems (IEEE AESS), and Reliability Societies. He earned his Ph.D. in Computer Science and Systems Engineering from Korea Aerospace University and his MSc and BEng in Mechatronics from Hanoi University of Science and Technology. His research focuses

on Dynamics and Control Theory, AI-based Digital Twin Systems, and Autonomous Intelligent Systems.



**Eunmi Choi** currently at Kookmin University, Korea, specialises in big data infrastructure, cloud computing, intelligent systems, information security, parallel and distributed systems, and software architecture. She earned her M.S. and Ph.D. in Computer Science from Michigan State University (1991, 1997) and her B.S. from Korea University (1988). Previously, she was an assistant professor at Handong University (1998-2004). She leads the Distributed Information System and Cloud Computing Lab at Kookmin University.